Available online at www.sciencedirect.com
SCIENCE DIRECT
Archives of Biochemistry and Biophysics 450 (2006) 191–202
ABB
www.elsevier.com/locate/yabbi

Cooperative unfolding of *Escherichia coli* ribosome recycling factor originating from its domain–domain interaction and its implication for function

Liqiang Zhang [a], Peng Guo [a], Hongjie Zhang [b,*], Guozhong Jing [a,*]

[a] *National Laboratory of Biomacromolecules, Institute of Biophysics, Chinese Academy of Sciences, China*
[b] *Center for Systems Biology, Institute of Biophysics, Chinese Academy of Sciences, China*

Received 6 February 2006, and in revised form 24 March 2006
Available online 18 April 2006

Abstract

Cooperative unfolding of *Escherichia coli* ribosome recycling factor (RRF) and its implication for function were investigated by comparing the in vitro unfolding and the in vivo activity of wild-type *E. coli* RRF and its temperature-sensitive mutant RRF_{V117D}. The experiments show that mutation V117D at domain I could perturb the domain II structure as evidenced in the near-UV CD and tyrosine fluorescence spectra though no significant globular conformation change occurred. Both equilibrium unfolding induced by heat or denaturant and kinetic unfolding induced by denaturant obey the two-state transition model, indicating V117D mutation does not perturb the efficient interdomain interaction, which results in cooperative unfolding of the RRF protein. However, the mutation significantly destabilizes the *E. coli* RRF protein, moving the thermal unfolding transition temperature range from 50–65 to 35–50 °C, which spans the non-permissive temperature for the growth of *E. coli* LJ14 strain (frr^{ts}). The in vivo activity assays showed that although V117D mutation results in a temperature sensitive phenotype of *E. coli* LJ14 strain (frr^{ts}), over-expression of mutant RRF_{V117D} can eliminate the temperature sensitive phenotype at the non-permissive temperature (42 °C). Taking all the results into consideration, it can be suggested that the mechanism of the temperature sensitive phenotype of the *E. coli* LJ14 cells is due to inactivation of mutant RRF_{V117D} caused by unfolding at the non-permissive temperatures.

Keywords: Ribosome recycling factor; Substitution mutation; Cooperative unfolding; In vivo activity assay

Protein synthesis consists of initiation, elongation, termination, and ribosome recycling. When translation of an mRNA has been completed on the ribosome, the peptidyl-tRNA with a nascent polypeptide is translocated into the ribosome P site, and a stop codon is translocated into the ribosomal A site. Then one of the class I release factors, RF1 or RF2, binds to the ribosomal A site and induces the release of the nascent polypeptide. Afterwards a class II release factor RF3 binds to the ribosome, catalyzes the release of RF1 or RF2, and dissociates in a GTP-dependent manner [1–3], leaving behind the post-termination ribosomal complex consisting of mRNA, deacylated tRNA in P site, and an empty A site. Disassembly of the post-termination complex, recycling of the ribosomal subunits back to a new round of initiation, is an essential step in protein synthesis. Ribosome recycling factor (RRF)[1] is essential for bacterial growth [4,5] and, in concert with elongation factor EF-G, triggers dissociation of the post-termination complex [6–9]. As an essential protein factor for protein synthesis in bacteria, all reported RRFs are highly similar in amino acid sequences [10,11]. Crystal and solution structures of RRF have been solved for six different bacterial species; all of these structures comprise

* Corresponding authors. Fax: +86 10 64840672.
E-mail addresses: hjzhang@sun5.ibp.ac.cn (H. Zhang), jinggzh@sun5.ibp.ac.cn (G. Jing).

[1] *Abbreviations used:* RRF, ribosome recycling factor; CD, circular dichroism; ASA, solvent-accessible surface area; Ts, temperature sensitive.

0003-9861/$ - see front matter © 2006 Elsevier Inc. All rights reserved.
doi:10.1016/j.abb.2006.03.029

two domains connected by a flexible hinge: domain I displays a three-stranded α-helix bundle structure, and domain II exists as a three layer β/α/β sandwich structure [10–16].

In recent years, extensive work has been done in studying the mechanism of the post-termination complex disassembly [9–11,17–24]. The studies showed that splitting of the post-termination ribosome into subunits is catalyzed by the concerted action of RRF and EF-G on the ribosome. Our recent study further indicated that domain II of RRF plays a crucial role in the concerted action of RRF and EF-G for the post-termination complex disassembly and domain I mainly contributes to ribosome binding of the RRF molecule [25]. However, researchers have not paid enough attention to studying the relation between structure and function of the RRF molecule itself. Crystal structure analysis of *Thermotoga maritime* RRF showed that the water-accessible surface area lost in domain–domain interaction is only 8.2% of the domain areas. The lower interface may indicate a weak interaction between the domains [12]. Results from the backbone dynamics of *Escherichia coli* RRF in water characterized by ^{15}N NMR relaxation analysis and molecular dynamics simulation also indicated that *E. coli* RRF has a characteristic two domain structure in solution and each structural domain behaves as a rigid body [26]. Examination of the crystal packing of *Mycobacterium tuberculosis* RRF revealed extensive contacts between domain I and the symmetry-related molecules. However, domain II makes fewer contacts with the symmetry mates, with a large channel of water molecules surrounding it. Consequently, while domain I is held rigid in crystal, domain II is afforded considerable conformational freedom [16]. Taken together, all these results assume that there is only a weak interaction between the two RRF domains, and the folding of domain I and domain II is relatively independent. However, crystal structure analysis of *Thermus Thermophilus* RRF revealed that although the hinge flexibility is vital for the function of RRF, the steric interaction between the hinge loop and domains I and II restricts the interdomain angle, and this interaction makes different RRFs have their specific interdomain angles [10]. This observation implied that interdomain interaction may play a certain role in RRF function. To clarify whether interdomain interaction exists in RRF molecules and what its implication for RRF function is, an *E. coli* RRF mutant, RRF_{V117D}, was chosen as a model. The reasons for choosing this mutant were threefold. Mutant V117D is located in α-helix 3 of RRF domain I (Fig. 1), which can be used as a probe to examine the interdomain interaction. Second, mutant V117D rends the *E. coli* RRF temperature sensitive. *E. coli* strain LJ14, which has only the chromosomal copy of the mutant V117D gene (*frr*^{ts}), can not grow at the non-permissive temperature. Third, although the RRF coded for by *frr*^{ts} (V117D) loses its ribosome-releasing activity upon exposure to an elevated temperature, there is residual RRF activity in vitro. An excess amount of the residual activity of mutant RRF_{V117D} expressed from the multicopy vector eliminates the temperature sensitive phenotype in vivo [4].

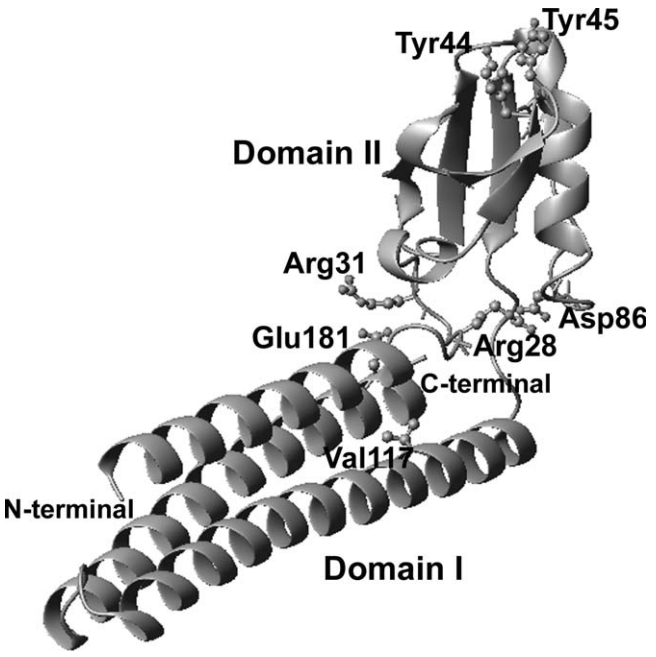

Fig. 1. Crystal structure of *E. coli* RRF mutant Arg132Gly using PDB ID: 1ISE.pdb. The graph was built using MolMol software. *E. coli* RRF consists of 185 amino acids with a molecular weight of 20,639. The RRF is an open L-shaped molecule composed of two domains connected by a flexible hinge. The first domain (residues 1–30 and 104–185) contains three α-helices, and the second domain (residues 32–102) contains one α-helix and six β-strands. The side chains of Arg28, Arg31, Tyr44, Tyr45 Asp86, Val117, and Glu181 are indicated. Note that the side chains of Tyr44 and Tyr45 at the domain II are highly exposed to solvent.

These properties of mutant RRF_{V117D} make it a good model for studying the thermal inactivation mechanism of *E. coli* RRF. In this paper, circular dichroism (CD) and intrinsic tyrosine fluorescence spectra were utilized to detect the structural characteristics of *Eco*RRF and its mutant RRF_{V117D} and to investigate the differences in their thermodynamic and kinetic stability. Furthermore, the thermal inactivation mechanism of RRF was also studied by comparing the thermal stability and the in vivo activity of *Eco*RRF and its mutant RRF_{V117D}. The results indicate that V117D substitution mutation significantly destabilizes the *Eco*RRF protein, moving the unfolding transition temperature ranges from 50–65 to 35–50 °C. However, the mutation does not perturb the efficient interdomain interaction, which results in cooperative unfolding of the RRF protein. The temperature sensitive phenotype of the *E. coli* LJ14 cells caused by V117D substitution is due to the cooperative unfolding of mutant RRF_{V117D} at the non-permissive temperatures.

Materials and methods

Bacterial strains, plasmids, and chemicals

Escherichia coli LJ14 is a MC1061 strain (*frr*^{ts}), of which the chromosomal wild-type *frr* allele is replaced with a mutant allele (V117D) [4], allowing *E. coli* LJ14 to grow at 30 °C but not at 42 °C. The strain was used for the in

vivo activity assays of *E. coli* wild-type RRF (*Eco*RRF) and mutant RRF_{V117D} by complementation analysis. *E. coli* BL21(DE3) plysS strain was used as a host cell for expression of *Eco*RRF and mutant RRF_{V117D}. pET-DB was constructed in our laboratory [27] and used for the expression of *Eco*RRF and mutant RRF_{V117D}. pQE-60 is a vector with a strong T_5 promoter purchased from QIAGEN. It was used to construct pQE-*Eco*RRF and pQE-RRF_{V117D} for analysis of the complementation of *E. coli* LJ14 (*frr*^{ts}). Restriction endonucleases were from NEB and the DNA ligation kit from Takara. All other reagents were of analytic grade.

Construction of plasmids for the expression of E. coli RRF and its mutant RRF_{V117D}

pQE-*Eco*RRF plasmid for the in vivo activity assay of *Eco*RRF was constructed as described [28]. For construction of pET-DB-*Eco*RRF, the *Eco*RRF coding sequence was obtained by digestion of pQE-*Eco*RRF plasmid with *Nco*I and *Bam*HI, and then the *Eco*RRF gene was inserted into the same sites of pET-DB, resulting in pET-DB-*Eco*RRF for expression of *Eco*RRF.

pET-DB-RRF_{V117D} for expression of mutant RRF_{V117D} was constructed by overlap extension [29]. Four primers were designed: forward (5′-GC AGC **TCC ATG GTT** AGC GAT ATC AGA AAA GAT GCT GAA GTA CG-3′) and reverse (5′-CTC GAG **AAG CTT** TCA GAA CTG CAT CAG TTC TG-3′) primers containing *Nco*I and *Hin*dIII cut sites (bold), and complementary mutant primes (5′-C TTC ACC ACG **ATC** GAT TTT GGT CAG-3′ and 5′-CTG ACC AAA ATC **GAT** CGT GGT GAA GC-3′) containing mutation sites (bold), respectively. Three polymerase chain reactions (PCRs) were performed using pQE-*Eco*RRF as a template. The PCR product was digested with *Nco*I and *Hin*dIII and then cloned into pET-DB and pQE-60, resulting in pET-DB-RRF_{V117D} and pQE-RRF_{V117D}, respectively. The authenticity of all the cloned genes was verified by DNA sequence analysis.

Expression and purification of E. coli RRF and its mutant RRF_{V117D}

Expression and purification of *E. coli* RRF and its mutant RRF_{V117D} were performed exactly as described in [28]. In brief, each plasmid was transformed into *E. coli* BL21 (DE3) pLysS cells. Fresh culture of transformant was induced with 0.5 mM IPTG, and the overproduced protein was purified by metal chelating affinity chromatography. Because twenty-two amino acid residues including a His_6-tag and a thrombin cleavage site were fused in-frame to the N-terminal end of each protein when its gene was cloned into pET-DB vector [27], each protein was first expressed as a His_6-tagged one. The purified fusion protein was then incubated with thrombin (Sigma T4648) in the ratio of 10 U of thrombin/milligram protein in cleavage buffer (20 mM Tris–HCl, pH 8.0, 2.5 mM $CaCl_2$, 10 mM $MgCl_2$) at 4 °C for 8 h. After digestion, the cleavage mixture was applied onto a Pharmacia Superdex 75 Hiload column, and then eluted with elution buffer (50 mM Tris–HCl, pH 7.5/100 mM NaCl/100 μM PMSF). The major peak of each protein was collected and dialyzed against 50 mM NH_4Cl at 4 °C. Finally, the purified proteins were lyophilized and stored at −20 °C. Each purified protein appeared as a single band on a 15% SDS–polyacrylamide gel. Protein concentrations were determined by absorbance measurements at 280 nm using absorption coefficients of $\varepsilon_{280nm}^{0.1\%,1cm} = 2680\ ml\ mg^{-1}\ cm^{-1}$. The coefficient was calculated from the amino acid compositions following the procedure described by Pace et al. [30].

In vivo assays for RRF activity

The in vivo assay was performed by monitoring complementation of the *E. coli* LJ14 (*frr*^{ts}) with *Eco*RRF and mutant RRF_{V117D}. Each plasmid (pQE-*Eco*RRF or pQE-RRF_{V117D}), which expresses *Eco*RRF or mutant RRF_{V117D}, was transformed into *E. coli* LJ14 (*frr*^{ts}). Cultures were started with a 0.06% (v/v) inoculums from freshly grown (at 30 °C) overnight cultures, and growth at both permissive (30 °C) and non-permissive (42 and 45 °C) temperatures was monitored by recording culture turbidities at 600 nm at regular intervals [31]. The expression level of RRFs was detected by immunoblotting using anti-*Eco*RRF antibodies and a SuperSignal West Pico Trial Kit (Pierce). Protein extracts were prepared from equal amounts of culture cells at different temperatures.

Circular dichroism (CD) spectra

Circular dichroism spectra of *Eco*RRF and mutant RRF_{V117D} were obtained at 25 °C using an Applied Photophysics PiStar-180 spectrometer with a 1-mm path length quartz cuvette. The protein concentration in the samples was 5 μM for far-UV CD (250–200 nm) and 200 μM for near-UV CD (320–250 nm), in 50 mM phosphate buffer, pH 7.5. The CD spectra data were taken at 1 nm intervals with an integration time of 1 s. The data represent the average of five scans after correction for the buffer baseline and were reported as mean residue ellipticity ($[\theta]$).

Intrinsic tyrosine fluorescence spectra

Intrinsic tyrosine fluorescence emission spectra of *Eco*RRF and mutant RRF_{V117D} were measured at 25 °C using a Hitachi F-4500 fluorescence spectrophotometer with a slit width of 5 nm. The excitation wavelengths were 280 nm and the concentration of each protein was 5 μM in 50 mM phosphate buffer, pH 7.5.

Thermal unfolding transitions

Thermal unfolding of *Eco*RRF and mutant RRF_{V117D} was monitored by CD signal changes at 222 and 277 nm,

respectively. Each sample contained 5 μM of protein in 50 mM phosphate buffer, pH 7.5. For heat induced denaturation, proteins were heated at 1 °C/min from 35 to 70 °C for *Eco*RRF and 20 to 55 °C for mutant RRF_{V117D} using the PC.2 Peltier temperature controller accessory of the PiStar-180 instrument. The cuvette (1 mm path length) was sealed with parafilm to prevent evaporation while the pressure was kept relatively constant.

The *van't Hoff* enthalpy and the midpoint temperatures of the CD transition curves were determined by simulation of the transition curves according to a two-state mechanism [32] using the following equations:

$$[\theta](T) = [\theta]_{Nb}(T) + ([\theta]_{Ub}(T) - [\theta]_{Nb}(T)) \cdot ((q(T) - 1)/q(T)) \quad (1)$$

$$[\theta]_{Nb}(T) = a + b \cdot (T - T_{\mathrm{m}}) \quad (2)$$

$$[\theta]_{Ub}(T) = c + d \cdot (T - T_{\mathrm{m}}), \quad (3)$$

where $[\theta]_{Nb}(T)$ is the temperature dependence of the native state baseline, and $[\theta]_{Ub}(T)$ is that of the unfolded state. Both were assumed to be linear.

$$q(T) = 1 + K(T) \quad (4)$$

is the partition function of a two-state transition involving the equilibrium constant $K(T)$.

The temperature dependence of the equilibrium constant depends on the standard Gibbs energy change ΔG^o for unfolding, which can be calculated from the experimental transition enthalpy ΔH^o and the transition temperature T_m according to

$$K(T) = \exp(-\Delta G^o/RT) \quad (5)$$

and

$$\Delta G^o = \Delta H^o \cdot (1 - T/T_{\mathrm{m}}). \quad (6)$$

The software of SigmaPlot 6.0 was used for the data analysis.

GdnHCl-induced equilibrium denaturation

GdnHCl-induced denaturation of *Eco*RRF and its mutant RRF_{V117D} was measured at 25 °C by monitoring the change in CD signal at 222 nm with a 1 mm path length quartz cuvette. Each sample contained 5 μM of protein in 50 mM phosphate buffer, pH 7.5, with different concentrations of GdnHCl and was incubated overnight at 25 °C before experiments. The data were obtained by the average of four scans. GdnHCl-induced denaturation of *Eco*RRF and mutant RRF_{V117D} was also monitored by using the change in intrinsic tyrosine fluorescence. Each sample contained 5 μM of protein in 50 mM phosphate buffer, pH 7.5, with different concentrations of GdnHCl at 25 °C as described above. The unfolding progress was determined by

$$f = \frac{y - y_N}{y_D - y_N}, \quad (7)$$

where y is the measured CD or fluorescence signal, y_N is the CD or fluorescence signal of RRF for the native state and y_D is that of the extrapolated value for the denatured state, assuming that they are linearly dependent on GdnHCl concentration, i.e.,

$$y_N = y_N^o + m_N[\mathrm{GdnHCl}] \quad (8)$$

and

$$y_D = y_D^o + m_D[\mathrm{GdnHCl}]. \quad (9)$$

Evaluation of the isothermal unfolding curves was performed numerically following the procedure of Santoro and Bolen [33] using two-state model equations through the software of SigmaPlot 6.0:

$$f = \frac{y_N + y_D Q}{1 + Q} \quad (10)$$

$$Q = \exp\left(-\frac{\Delta G_D^o(\mathrm{H_2O}) - m_G[\mathrm{GdnHCl}]}{RT}\right), \quad (11)$$

where $\Delta G_D^o(\mathrm{H_2O})$ is the standard Gibbs free energy change for unfolding in the absence of denaturant, and m_G is the slope of the plot of $\Delta G_{\mathrm{app}}^o$ versus denaturant concentration, according to

$$\Delta G_{=}\Delta G_D^o(\mathrm{H_2O}) - m_G[\mathrm{GdnHCl}]. \quad (12)$$

GdnHCl-induced unfolding kinetics

Unfolding kinetics of *Eco*RRF and mutant RRF_{V117D} were monitored at the CD signal at 225 nm by fast mixing of the RRF sample from one syringe and concentrated GdnHCl solution from a secondary syringe by 1:10 dilution using an Applied Photophysics stopped-flow apparatus. The reason for selecting 225 nm was just due to the better signal/noise ratios compared to that at 222 nm. The final concentration of each protein was 10 μM. The unfolding kinetics was analyzed using the first-order kinetic process equation

$$[\theta]_t = [\theta]_0 + ([\theta]_\infty - [\theta]_0) \cdot \exp(-k_u t), \quad (13)$$

where $[\theta]_t$ indicates the measured CD signal at 225 nm at time t after mixing RRF with GdnHCl; $[\theta]_0$ is the CD signal of protein without denaturant; and $[\theta]_\infty$ is the CD signal of protein at a certain concentration of GdnHCl to the equilibrium state. k_u refers to the unfolding rate constant at a certain concentration of denaturant.

Plots of $\ln k_u$ versus the denaturant concentrations are linear in the post transition region, and $\ln k_u(\mathrm{H_2O})$ could be linearly extrapolated to the zero concentration of denaturant [34] according to equation

$$\ln k_u = \ln k_u(\mathrm{H_2O}) + \frac{m_u}{RT} \cdot [\mathrm{denaturant}], \quad (14)$$

where mr_u/RT indicates the slope of the unfolding rate constant versus denaturant concentrations.

The free energies of activation for the unfolding ($\Delta G_u^{0\neq}$) were calculated using the transition state theory according to Eyring [35]

$$\ln k_u(H_2O) = \ln\frac{\kappa k_b T}{h} - \frac{\Delta G_u^{0\neq}(H_2O)}{RT}, \quad (15)$$

where k_b is the Boltzmann constant, T is the absolute temperature in Kelvin, h is the Planck constant, R is the gas constant, and κ is the transmission factor which is arbitrarily set as unity.

Results

Effect of V117D mutation on the CD spectra of E. coli RRF

Far-UV CD spectra were used to assess the secondary structure, especially the α-helical content. The appearance of two negative peaks at 208 and 222 nm in the CD spectrum is usually considered to be indicative of the content of α-helical structure in a protein [36,37]. Fig. 2A shows the far-UV CD spectra of *Eco*RRF and mutant RRF_{V117D}. The double negative peaks centered at 208 and 222 nm remained with slight decrease of the signal (8%) caused by V117D substitution, indicating that mutation has no significant effect on the secondary structure of the protein. The CD spectrum of a protein in the near-UV spectral region (350–250 nm) can be sensitive to certain aspects of tertiary structure, which reflect the asymmetry of the environment of aromatic amino acid residues [36,37]. Fig. 2B shows the near-UV CD spectra of *Eco*RRF and mutant RRF_{V117D}. Compared with *Eco*RRF, the $[\theta]_{277nm}$ value of mutant RRF_{V117D} is decreased by 47%. There are three aromatic residues (F_{20}, Y_{44}, and Y_{45}) in the proteins and both of the two tyrosine residues are located at domain II. Since, signals from 270–290 nm are attributable to tyrosine and since the CD spectrum of a protein in the near-UV spectral region can be sensitive to small changes in tertiary structure, this change at 277 nm indicates that the V117D substitution significantly perturbs the local conformation surrounded by the two residues, suggesting that mutation of V117D at domain I could result in structural perturbation at the RRF domain II.

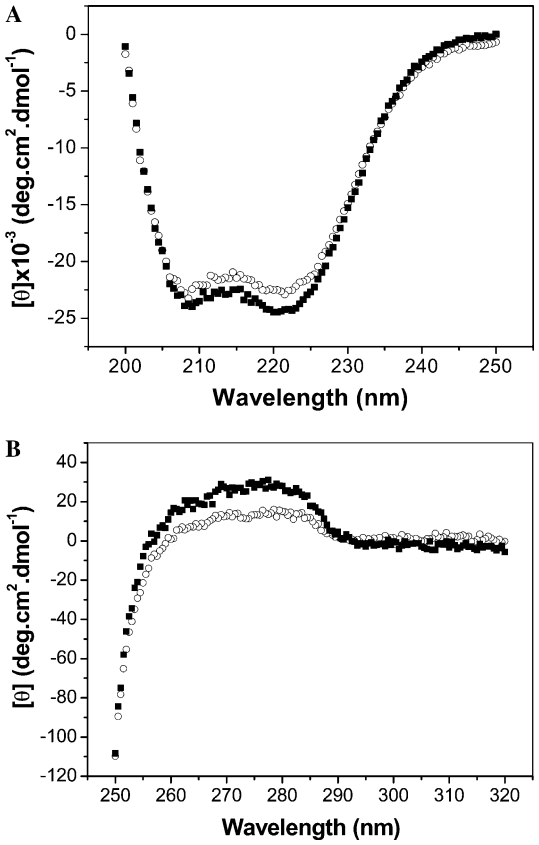

Fig. 2. CD spectra of *Eco*RRF and its mutant RRF_{V117D}. (A) Far-UV CD spectra of *Eco*RRF (■) and its mutant RRF_{V117D} (○). (B) Near-UV CD spectra of *Eco*RRF (■) and its mutant RRF_{V117D} (○). The spectra were obtained at 25 °C; the detailed experimental conditions are described in the text.

Effect of V117D mutation on the intrinsic fluorescence spectra of E. coli RRF

There are only two tyrosine residues in the RRF molecule, which are located at positions 44 and 45 (Y_{44} and Y_{45}) at domain II of RRF [13]. Changes in the intrinsic tyrosine fluorescence spectra after excitation at 280 nm reflect the changes in the local environment of the tyrosine residues. Fig. 3 shows the tyrosine emission spectra of *Eco*RRF and mutant RRF_{V117D}. Compared with the fluorescence emission spectrum of *Eco*RRF, there is an increase in fluorescence intensity for mutant RRF_{V117D}, indicating that V117D substitution has some effect on the local environment of the tyrosine residues in the protein. However, the fluorescence intensity for both *Eco*RRF and mutant RRF_{V117D} is much lower than at 2 M

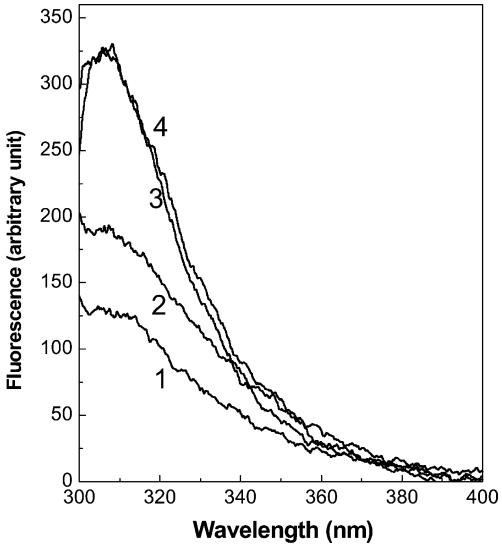

Fig. 3. Tyrosine fluorescence emission spectra of *Eco*RRF and its mutant RRF_{V117D}. Lines 1 and 2 denote the spectra of *Eco*RRF and its mutant RRF_{V117D} in 50 mM phosphate buffer, pH 7.5, 25 °C, respectively; lines 3 and 4 denote the spectra of *Eco*RRF and its mutant RRF_{V117D} in the phosphate buffer containing 2 M GdnHCl, respectively. The protein concentrations were of 5 μM.

GdnHCl, at which concentration both of the proteins are unfolded. This result shows that the intrinsic tyrosine fluorescence for both *Eco*RRF and mutant RRF_{V117D} is quenched somewhat though V117D substitution suppresses the intrinsic tyrosine fluorescence quenching to some extent. This observation also suggests that V117D mutation at domain I perturbs the local environment of the tyrosine residues at domain II. It is noteworthy that since the tyrosine side chains are highly exposed to solvent in the native conformation as shown in Fig. 1, the fluorescence quenching is weaker for these tyrosines in its unfolded state denatured by GdnHCl, which could account for the apparent increase of fluorescence during protein unfolding as shown later in Fig. 6B.

Effect of V117D mutation on thermal stability of E. coli RRF

Thermal unfolding of *Eco*RRF and mutant RRF_{V117D} was measured by monitoring changes in the far-UV CD spectra at 222 nm as described in Materials and methods, which reflects RRF's secondary structure unfolding. To test their folding reversibility, reheating of the same samples with the same heating rate was performed just after the temperature of the heated samples reached their beginning temperature as shown in Fig. 4. The results indicate that both *Eco*RRF and mutant RRF_{V117D} could fold reversibly, at least partially. Thus thermodynamic analysis method could be applied to the unfolding process of this system [38,39]. For convenient comparison with the unfolding transitions monitored by near-UV CD at 277 nm, the thermal unfolding diagrams of their secondary structures were shown in the fraction of unfolded RRF versus temperature after linear baseline correction (Fig. 5). The thermal unfolding transitions for both *Eco*RRF and mutant RRF_{V117D} are single sigmoidal ones, indicating that their thermal unfolding processes obey the two-state transition model. The only difference between *Eco*RRF and mutant RRF_{V117D} is that mutation of V117D significantly destabilizes the protein. Thermal unfolding for *Eco*RRF began at about 50 °C and finished at about 65 °C. In contrast, unfolding for RRF_{V117D} began at about 35 °C and finished at about 50 °C. Special attention was given at temperatures of 30, 42, and 45 °C correspondingly, the unfolded fraction for *Eco*RRF was zero at all three temperatures, while for mutant RRF_{V117D}, it was zero, 30 and 63%, respectively. Thermodynamic parameters of enthalpies and transition temperatures were determined by numerically fitting the experimental data from Eqs. (1) – (6) and the results are listed in Table 1. The *van't Hoff* enthalpy for *Eco*RRF is 445 kJ mol^{-1} and for RRF_{V117D} is 351 kJ mol^{-1}. The transition temperature for *Eco*RRF is 59.6 °C and for mutant RRF_{V117D} is 45.2 °C. Clearly, from the thermodynamic point of view, the destabilization caused by V117D mutation is mostly due to decreasing the packing energy of the RRF molecule.

Thermal unfolding of *Eco*RRF and mutant RRF_{V117D} was also measured by monitoring changes in the near-UV

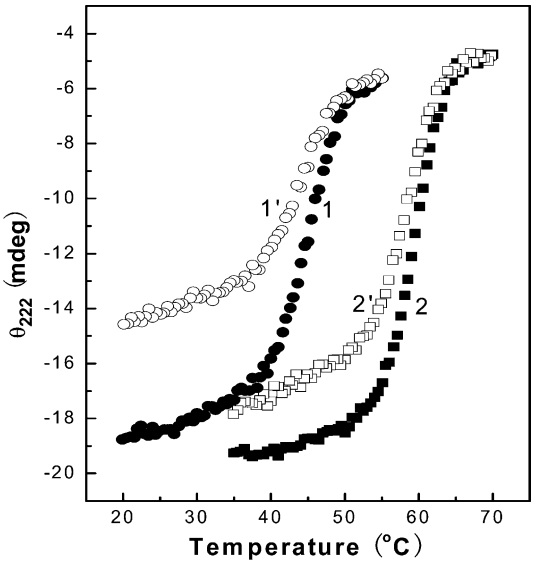

Fig. 4. Thermal unfolding reversibility of *Eco*RRF and its mutant RRF_{V117D}. Thermal unfolding of *Eco*RRF and mutant RRF_{V117D} was monitored by CD signal changes at 222 nm. Each sample contained 5 μM of protein in 50 mM phosphate buffer, pH 7.5. The solid signals 1 (●) and 2 (■) denote the first scan of *Eco*RRF and its mutant RRF_{V117D}, respectively, with the scan rate of 1 °C/min and the open signals 1′ (○) and 2′ (□) denote the corresponding second scans after the heated sample cooling to their beginning temperatures.

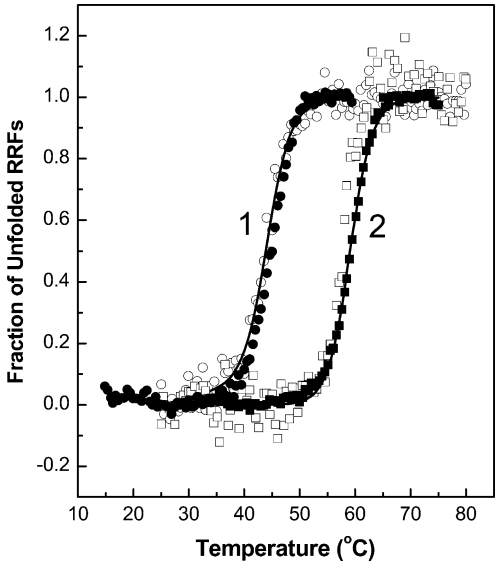

Fig. 5. Thermal unfolding transitions of *Eco*RRF and its mutant RRF_{V117D}. Thermal unfolding of *Eco*RRF and its mutant RRF_{V117D} was monitored by CD signal changes at 222 and 277 nm, respectively. Each sample contained 5 and 200 μM of protein in 50 mM phosphate buffer, pH 7.5, for far-UV CD measurements and for near-UV CD measurements, respectively. Filled squares (■) and circles (●) denote the thermal unfolding of *Eco*RRF and its mutant RRF_{V117D} monitored by CD signal changes at 222 nm, respectively. Open squares (□) and circles (○) denote the thermal unfolding of *Eco*RRF and its mutant RRF_{V117D} monitored by CD signal changes at 277 nm, respectively. The solid lines represent the best fitting of the data according to the two-state model. The detail experimental conditions are described in the text.

Table 1
Thermodynamic parameters of WT and mutant RRF_{V117D} during their thermal unfolding

Protein	ΔH (kJ mol^{-1})	T_m (°C)
WT RRF	445 ± 10	59.65 ± 0.07
RRF_{V117D}	351 ± 9	45.22 ± 0.08

CD spectra at 277 nm, which mainly reflects RRF's local structure change surrounding the tyrosine residues in domain II. The fraction of unfolded RRF versus temperature is also shown in Fig. 5. The thermal unfolding of *Eco*RRF and mutant RRF_{V117D} monitoring by far-UV CD at 222 nm and near-UV CD at 277 nm are overlapped with each other. The superimposing of the secondary structure change dominated by domain I with the local structure change dominated by domain II indicates that unfolding of domain I and domain II are cooperative.

GdnHCl-induced isothermal unfolding of E. coli RRF and mutant RRF_{V117D}

GdnHCl-induced globular unfolding of *Eco*RRF and mutant RRF_{V117D} was further measured at 25 °C by monitoring changes in the far-UV CD spectra at 222 nm. Fig. 6A shows the equilibrium unfolding transition progress in a series of GdnHCl concentrations, where the native states were set as zero and the fully unfolded states at 2 M were set as unity. Refolding of the *Eco*RRF and mutant RRF_{V117D} was also monitored under the same conditions. The refolding transition curves for *Eco*RRF and mutant RRF_{V117D} were shown to superimpose their unfolding transition curves, respectively. These results indicate that unfolding for both *Eco*RRF and mutant RRF_{V117D} induced by GdnHCl is reversible. The GdnHCl-induced unfolding transition curves for both *Eco*RRF and mutant RRF_{V117D} are also single sigmoidal ones, indicating that the unfolding processes are cooperative and obey the two-state transition model.

Fig. 6B shows the GdnHCl-induced unfolding transition of *Eco*RRF and mutant RRF_{V117D} monitored by intrinsic tyrosine fluorescence intensity at 306 nm. Both of them give a single sigmoidal transition and also obey the two-state unfolding model. The thermodynamic parameters of the standard Gibbs free energies ($\Delta G^o_{H_2O}$) and m_G values were obtained by numerically fitting the data to from Eqs. (7) – (12), and the results are listed in Table 2. The $\Delta G^o_{H_2O}$ for *Eco*RRF was 22.0 ± 2.7 and 28.6 ± 2.2 kJ mol^{-1} monitored by far-UV CD and intrinsic tyrosine fluorescence, respectively. The $\Delta G^o_{H_2O}$ for mutant RRF_{V117D} was 9.7 ± 2.1 and 7.6 ± 2.3 kJ mol^{-1}, respectively. These results indicate that the mutation of V117D results in a significant loss of stability. The similar values of $\Delta G^o_{H_2O}$ measured by far-UV CD and intrinsic tyrosine fluorescence further confirm the cooperative unfolding of the RRF molecules. The m_G values, the slope of free energies versus denaturant concentrations, for both *Eco*RRF and mutant RRF_{V117D} are the same within experimental errors (Table 2), providing further evidence that mutation has no significant perturbation effect on its solvent-accessible surface area (ASA) change [40], and thus no significant perturbation effect on its tertiary structure packing, provided the ASA difference caused by V117D mutation in their fully unfolded states could be ignored. The C_m values, the concentration of GdnHCl at which half of the protein molecules are denatured, were also calculated from Eq. (12) by setting $\Delta G = 0$, and the results are listed in Table 2. The C_m values for *Eco*RRF and mutant RRF_{V117D} were 0.92 and 0.38 M, respectively. These data further confirm that mutation of V117D can significantly destabilize the protein stability.

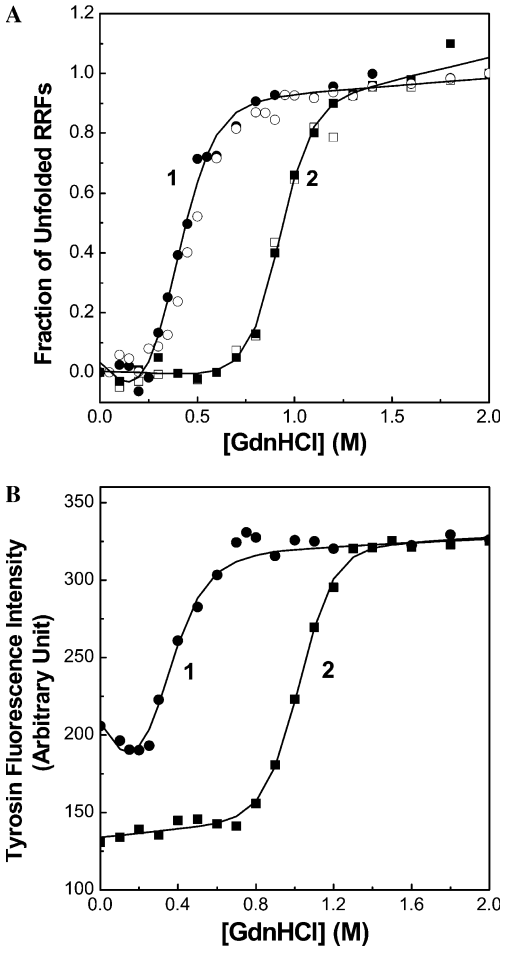

Fig. 6. GdnHCl-induced unfolding transitions of *Eco*RRF and its mutant RRF_{V117D}. The detail experimental conditions are described in the text. (A) GdnHCl-induced unfolding of *Eco*RRF and mutant RRF_{V117D} was monitored by CD signal changes at 222 nm The filled squares (■) and circles (●) denote the isothermal unfolding of *Eco*RRF and its mutant RRF_{V117D}, respectively. The open squares (□) and circles (○) denote the corresponding refolding of the thoroughly unfolded *Eco*RRF and its mutant RRF_{V117D} at 6 M GdnHCl overnight. (B) GdnHCl-induced unfolding of *Eco*RRF and mutant RRF_{V117D} monitored by intrinsic tyrosine emission fluorescence intensity at 306 nm, using the excitation at 280 nm. The filled squares (■) and circles (●) denote the isothermal unfolding of *Eco*RRF and its mutant RRF_{V117D}, respectively. The solid lines represent the best fitting of the data according to the two-state model.

Table 2
Thermodynamic parameters of WT and mutant RRF_{V117D} during their isothermal unfolding

Protein	Method	$\Delta G°$ (kJ mol^{-1})	m_G (kJ mol^{-1} M^{-1})	C_m (M)
WT RRF	Far-UV CD	22.0 ± 2.7	24.0 ± 2.7	0.92
	Tyr fluorescence	28.6 ± 2.2	27.9 ± 2.1	1.03
RRF_{V117D}	Far-UV CD	9.7 ± 2.1	25.7 ± 3.4	0.38
	Tyr fluorescence	7.6 ± 2.3	24.5 ± 3.7	0.31

Note. C_m is calculated from Eq. (12) using $\Delta G = 0$.

Unfolding kinetics of EcoRRF and mutant V117D monitored by secondary structure changes

Unfolding kinetic processes of *Eco*RRF and mutant RRF_{V117D} were investigated by monitoring the CD signal changes at 225 nm as shown in Fig. 7A. At 2 M GdnHCl, unfolding data of *Eco*RRF could be fitted with a single phase process using Eq. (13). The unfolding rate constant was determined as 0.505 s^{-1}. Unfolding rate constants of *Eco*RRF at 1.5, 2.5, and 3.0 M were 0.1126, 1.845, and 8.591 s^{-1}, respectively. The rate constants in the logarithm were plotted versus denaturant GdnHCl concentrations and are shown in Fig. 7B. Higher concentration of denaturant leads to much faster unfolding. The experimental points can be fitted linearly according to Eq. (14) with the unfolding rate constant of 1.56×10^{-3} s^{-1} (i.e., $\ln k_u(H_2O) = -6.46$) in buffer and the m_u, the slope of $\ln k_u$ versus denaturant concentration divided by RT, of 7.09 kJ mol^{-1} M^{-1}. Correspondingly the activation free energy of unfolding in buffer was calculated as 88.9 kJ mol^{-1} according to Eq. (15), where the parameter κ was set as one. Mutation of V117D made the RRF molecule unstable with a faster unfolding rate. Its unfolding kinetics is shown in the inset plot of Fig. 7A with the rate constant of 0.98 s^{-1} at 0.8 M GdnHCl. The denaturant concentration dependence of its unfolding rate constant in a logarithm is shown in Fig. 7B. The kinetic parameters of k_u (H_2O) in buffer was determined as 1.47×10^{-3} s^{-1} (i.e., $\ln k_u(H_2O) = -6.52$) and m_u as 20.1 kJ mol^{-1} M^{-1} by linear regression analysis of these data. Correspondingly the activation free energy of mutant unfolding in buffer was calculated as 89.1 kJ mol^{-1} according to Eq. (15), using the same parameter $\kappa = 1$. These results (Table 3) indicate clearly that both *Eco*RRF and mutant RRF_{V117D} unfold with a first-order kinetic process. The unfolding rates of *Eco*RRF and mutant RRF_{V117D} in pure buffer are the same within measurement error ranges, but their denaturant dependence is different. Mutant RRF_{V117D} is more sensitive to GdnHCl than wild-type RRF. These results indicate that although mutation of V117D does not significantly change the folded conformation of RRF, it significantly moves the unfolding transition state from a native-like state ($1 - m_u/m = 1 - 7.09/23.9 = 70\%$ native-like) to an unfolded-like state ($1 - m_u/m = 1 - 20.1/25.7 = 22\%$ native-like) in the denaturant-induced unfolding process [41].

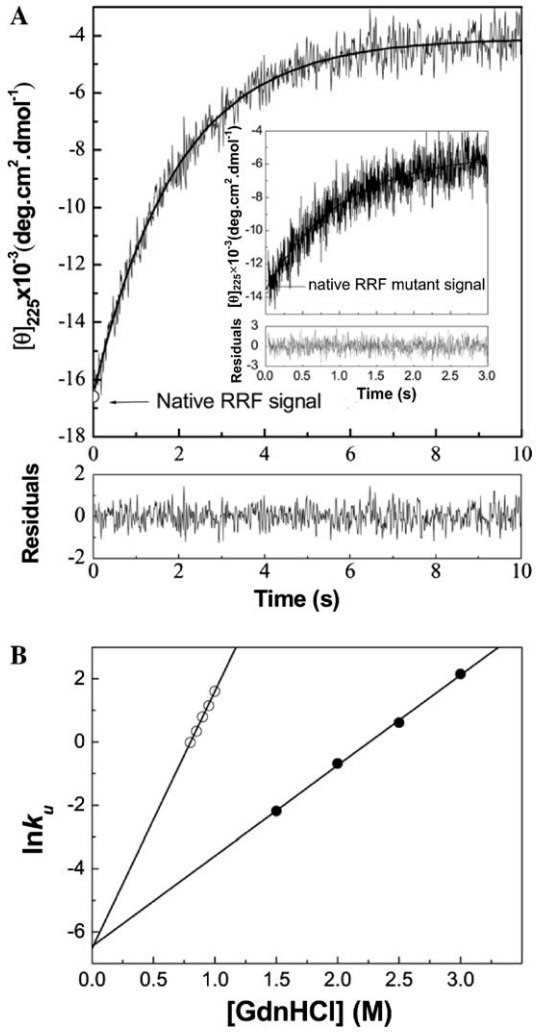

Fig. 7. Unfolding kinetics of *Eco*RRF and mutant RRF_{V117D} monitored by secondary structure changes. (A) Unfolding kinetic processes of *Eco*RRF and mutant RRF_{V117D} (in the inset). (B) The denaturant (GdnHCl) concentration dependence of unfolding rate constant of *Eco*RRF (●) and mutant RRF_{V117D} (○). The data were fitted linearly. The detailed experimental conditions are described in the text.

Over-expression of mutant RRF_{V117D} can rescue the temperature sensitive phenotype of E. coli LJ14 (frr^{ts})

The *E. coli* LJ14 strain is the most clear-cut temperature sensitive (Ts) mutant, of which the chromosomal wild-type

Table 3
Unfolding kinetic parameters of WT and mutant RRF_{V117D}

Protein	m_u (kJ mol^{-1} M^{-1})	k_u (H_2O)(s^{-1})	$\Delta G^{0\neq}$ (kJ mol^{-1})
WT RRF	7.09 ± 0.15	$1.56. \times 10^{-3}$	88.9
RRF_{V117D}	20.1 ± 0.32	1.47×10^{-3}	89.1

frr allele is replaced with a mutant allele (*frr*^{ts}, V117D), allowing *E. coli* LJ14 to grow at the permissive temperature (30 °C) but not at the non-permissive temperature (42 °C). Because of this, the strain is widely used for the in vivo activity assay of RRF by complementation analysis [25,31]. Janosi et al. [4] showed that an excess amount of the residual activity of mutant RRF_{V117D} expressed from multicopy pUC19 eliminated the temperature sensitive phenotype, suggesting a gene dosage effect. To clarify what is the mechanism of the temperature sensitive phenotype of mutant RRF_{V117D} and why high gene dosage can eliminate the temperature sensitive phenotype, an in vivo activity assay of mutant RRF_{V117D} was performed by monitoring the complementation of the *E. coli* LJ14 (*frr*^{ts}) with mutant RRF_{V117D}, and the expression level of the mutant at different temperatures was also analyzed as described in Materials and methods. As shown in Fig. 8A, at 30 °C, transformants harboring pQE-*Eco*RRF or pQE-RRF_{V117D} grew at almost the same rate as those harboring the vector pQE-60 alone, suggesting that the expression of these RRFs was not toxic to *E. coli*. Fig. 8B shows the growth rate of the transformants at 42 °C; all the transformants also grew well except that the growth of transformants harboring pQE-RRF_{V117D} was delayed for two hours. However, at 45 °C, the transformants harboring pQE-*Eco*RRF grew well, while those harboring either the vector pQE-60

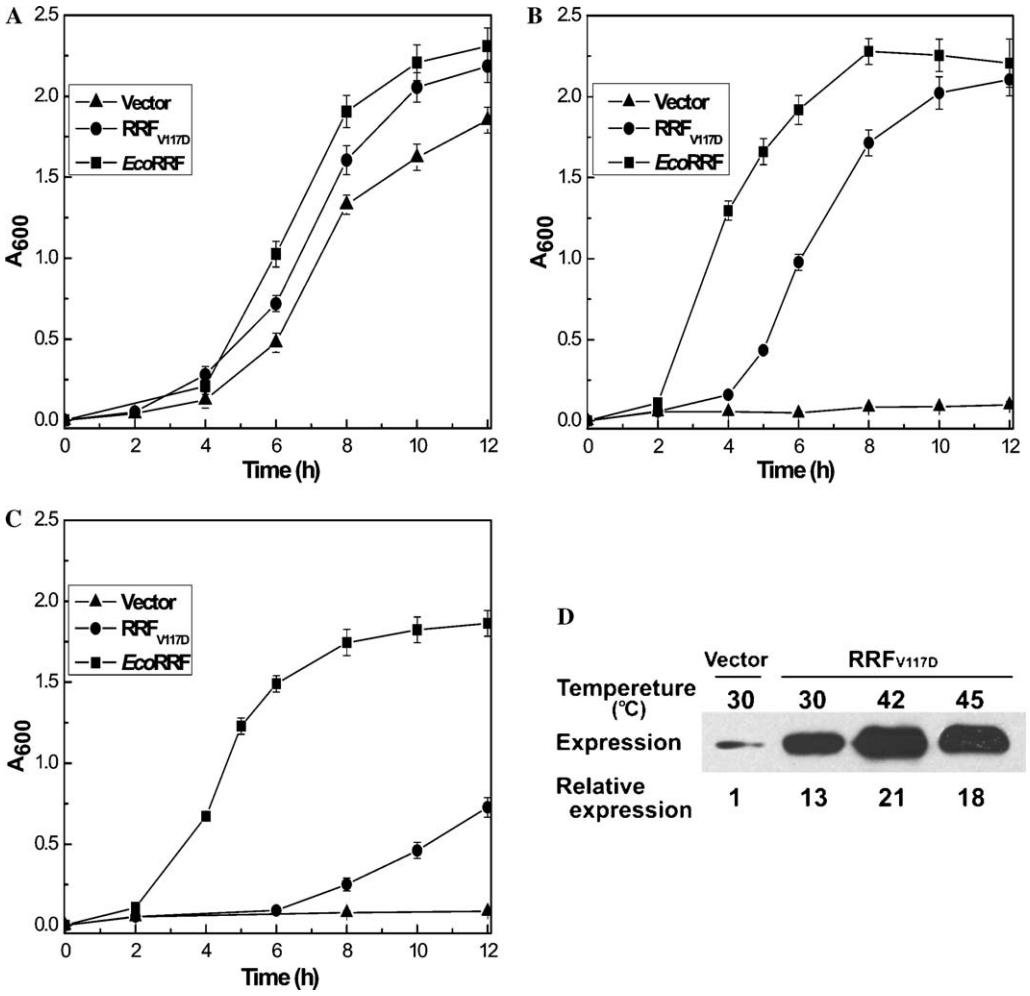

Fig. 8. In vivo activity assays of *Eco*RRF and its mutant RRF_{V117D} at different temperatures. The *E. coli* LJ14 (*frr*^{ts}) strain was transformed with the respective plasmids and examined for growth-phenotype. (A) Growth curves of various transformants of *E. coli* LJ14 (*frr*^{ts}) at the permissive temperature (30 °C). Vector, transformants with pQE-60; RRF_{V117D}, transformants with pQE-RRF_{V117D}; *Eco*RRF, transformants with pQE-*Eco*RRF. (B) Growth curves of various transformants of *E. coli* LJ14 (*frr*^{ts}) at the non-permissive temperature (42 °C). The transformants are the same as that indicated in (A). (C) Growth curves of various transformants of *E. coli* LJ14 (*frr*^{ts}) at the non-permissive temperature (45 °C). The transformants are the same as that indicated in (A). (D) Detection of mutant RRF_{V117D} expression in *E. coli* LJ14 (*frr*^{ts}) at different temperatures by immunoblotting using anti-*Eco*RRF antibodies. Protein extracts were prepared from equal amount of transformant cells harbouring pQE-60 or pQE-RRF_{V117D} at different temperatures after incubation for 12 h. The detailed experimental conditions are described in the text.

or pQE-RRF_{V117D} did not. The growth of transformants harboring pQE-RRF_{V117D} was significantly delayed (Fig. 8C). It is noteworthy that slow growth of the transformants harboring pQE-RRF_{V117D} was observed after prolonged incubation at 45 °C, suggesting that weak residual activity still remains in mutant RRF_{V117D} at 45 °C. The expression level of mutant RRF_{V117D} at different temperatures is shown in Fig. 8D. It can be seen that the amount of mutant RRF_{V117D} expressed in the *E. coli* LJ14 cells harboring pQE-RRF_{V117D} at 30, 42, and 45 °C is about 13, 21, and 18 times more than that of mutant V117D expressed by *E. coli* LJ14 cells (frr^{ts}) itself. The above thermal unfolding studies in vitro indicate that the heating temperatures at 42 and 45 °C for mutant RRF_{V117D} are just located in its thermal unfolding transition temperature range; and its unfolded fractions at 30, 42, and 45 °C are zero, 30 and 63%, respectively (Fig. 5). Thus the residual activity of mutant RRF_{V117D} expressed in the *E. coli* LJ14 cells harboring pQE-RRF_{V117D} at 42 and 45 °C would be enough for suppression of the temperature sensitive growth phenotype of *E. coli* LJ14 (frr^{ts}). These results may explain why high gene dosage can eliminate the temperature sensitive phenotype of the *E. coli* LJ14 cells. The mechanism of the temperature sensitive phenotype of the *E. coli* LJ14 cells is due to inactivation of mutant RRF_{V117D} caused by unfolding at the non-permissive temperatures. Of course, the in vitro thermal unfolding results could not exactly represent the state of the mutant RRF_{V117D} molecules in the bacterial cells and could not perfectly explain why the growth of transformants harboring pQE-RRF_{V117D} was significantly delayed at 45 °C, at which temperature about 37% of mutant RRF_{V117D} still remained folded (Fig. 5). A reasonable explanation may be that the growth of the *E. coli* LJ14 cells harboring pQE-RRF_{V117D} not only depends on the presence of RRF, but also is related to other proteins which may be inactivated at 45 °C.

Discussion

As described in the results section, although V117D substitution at domain I has no significant effect on the secondary structure of the RRF protein characterized by far-UV CD spectra (Fig. 2A), the mutation caused a decrease in the $[\theta]_{277nm}$ value of 47% (Fig. 2B). This observation indicates that V117D mutation at domain I significantly perturbs the specific packing of tyrosine residues in the tertiary structure of mutant RRF_{V117D}. Since all the tyrosine residues are located at domain II, the change in $[\theta]_{277nm}$ value indicates that mutation of V117D at domain I could result in the structural perturbation at the RRF domain II. This result was further confirmed by intrinsic tyrosine fluorescence spectra (Fig. 3). Taken together, the above results suggest the existence of interdomain interaction in the RRF protein. To know to what extent the interdomain interaction affects protein folding, the unfolding transition processes of *Eco*RRF and mutant RRF_{V117D} induced by both heat and GdnHCl were compared. Equilibrium unfolding of *Eco*RRF and mutant RRF_{V117D} monitored by using a far-UV CD signal at 222 nm showed a two state unfolding transition in both the isothermal-unfolding and thermal unfolding processes, suggesting that the unfolding of *E. coli* RRF domain I and domain II seems to be cooperative (Fig. 5). However, three questions should be addressed before making the final conclusion. Since there is about 90% content of α-helical structure in domain I, while domain II may be signal silent when using the signal probe of θ_{222nm}, the first question is whether the changes in θ_{222nm} reflect the unfolding process of the whole RRF molecule, not just the unfolding process of domain I. To verify this, the thermal unfolding of RRF monitored by the near-UV CD signal at 277 nm, which is dominated by the local structure of aromatic residues at domain II, was also performed. As shown in Fig. 5, excellent superimposition of the unfolding transitions monitored by both far-UV CD signal at 222 nm and near-UV CD signal at 277 nm indicates that the unfolding of domain I and domain II are cooperative. This consistency demonstrates that the unfolding transition of RRF monitored by the CD signal at 222 nm could reflect the conformation transition of the whole RRF molecule including domain II. These results were further confirmed by GdnHCl-induced isothermal unfolding monitored by both far-UV CD and intrinsic tyrosine fluorescence spectra (Fig. 6A and B). The second question is that even if the equilibrium unfolding of RRF is cooperative, its unfolding kinetics may be complicated. Therefore kinetic processes of unfolding of *Eco*RRF and mutant RRF_{V117D} were investigated by monitoring the signal changes of $[G]_{225nm}$. The results clearly indicate that both *Eco*RRF and mutant RRF_{V117D} unfold with a first-order kinetic process, suggesting that the unfolding of domain I and domain II of RRF is a simple two-state cooperative process (Fig. 7). The third question is whether the observed unfolding cooperativity is due to the same intrinsic stability of domain I and domain II in the RRF protein. In fact, this possibility does not exist. As indicated previously, domain I plays a major role in maintaining the stability of the RRF molecules [28]. *Tte*DI/*Eco*DII is a chimeric RRF in which domain I and domain II are from *Thermoanaerobacter tengcongensis* and *E. coli*, respectively. Since the unfolding of chimeric *Tte*DI/*Eco*DII RRF showed a three-state unfolding [28], the stability of each domain was estimated. The stability of 12.5 ± 2.2 kJ/mol for unfolding of *Eco*RRF domain II is much lower than the stability of 22.0 ± 2.7 kJ/mol for unfolding of *Eco*RRF as a whole. This result not only indicates the difference in the stability between the two domains, but also suggests the existence of interdomain interaction. Thus the intrinsic stability of domain II itself should be lower than the obtained value from chimeric *Tte*DI/*Eco*DII RRF domain II unfolding. Recently, a study from Nakano et al. [11] demonstrated that *Vibrio parahaemolyticus* RRF's domain I coding sequence could be solubly expressed in *E. coli*, while its domain II coding sequence could not, and the

observed *V. parahaemolyticus* domain II polypeptide was precipitated in the *E. coli* cells. In contrast, two RRF chimeras, *Eco*DI/*Tte*DII and *Tte*DI/*Eco*DII, created by domain swaps between the proteins from *E. coli* and *T. tengcongensis* were expressed in a soluble form [25,28]. These observations further suggest the intrinsic stability of domain II may be too low to keep itself folded correctly, and an efficient interaction between domain I and domain II of the RRF protein is crucial for the correct folding of the RRF molecules. It is the efficient interaction that results in cooperative unfolding of the *E. coli* RRF proteins.

The Crystal structure of *E. coli* mutant RRF_{R132G} (PDB ID: 1ISE) was analyzed. As shown in Fig. 1, there are 3 hydrogen bonds/electrostatic interactions (R28NE···D86OD1, R28NH2···D86OD2, and R31NE···E181OE1) between the domain I and domain II of the RRF protein. The distances between R28NE···D86OD1, R28NH2···D86OD2, and R31NE ···E181OE1 are 2.734, 3.325, and 2.915 Å respectively. It is noteworthy that similar hydrogen bonds between domain I and domain II of *V. parahaemolyticus* RRF has been reported by Nakano et al. [11]. The existence of these hydrogen bonds/electrostatic interactions between the two domains may play a significant role in the interdomain interaction of the RRF proteins.

Although the V117D substitution significantly perturbs the local conformation surrounded by the two tyrosine residues, the cooperative unfolding of mutant RRF_{V117D} during heat or GdnHCl induced denaturation indicates that V117D mutation does not perturb the efficient interdomain interaction of the mutant protein. Considering mutant RRF_{V117D} has almost the same activity as wild-type *Eco*RRF in the in vivo activity assay at the permissive temperature (Fig. 8A), the V117D substitution does not perturb the suitable conformation of the mutant RRF_{V117D} which is necessary for performing its function at the permissive temperature (30 °C). However, mutation of V117D significantly destabilizes the RRF protein as described above. The thermal unfolding study clearly indicates that the unfolding transition temperature range is moved from 50 to 65 °C for the wild-type RRF to the lower temperature range of 35–50 °C for the mutant RRF_{V117D} (Fig. 5). The non-permissive temperatures (42 and 45 °C), which were used for the in vivo activity assay of mutant RRF_{V117D}, are located within the unfolding transition region (Fig. 5). According to the two-state unfolding model, only native and fully unfolded mutant RRFs coexist at this temperature region. Since the amount of mutant RRF_{V117D} expressed in the *E. coli* LJ14 cells harboring pQE-RRF_{V117D} at 42 and 45 °C is about 21 and 18 times more than that of mutant RRF_{V117D} expressed by *E. coli* LJ14 cells (frr^{ts}) itself. According to the thermal unfolding transition of mutant RRF_{V117D}, the native fraction of mutant RRF_{V117D} at 42 and 45 °C should be 70 and 37%, respectively (Fig. 5). Thus the residual activity of mutant RRF_{V117D} expressed in the *E. coli* LJ14 cells harboring pQE-RRF_{V117D} at 42 and 45 °C would be enough for suppression of the temperature sensitive growth phenotype of *E. coli* LJ14 (frr^{ts}). These results may explain why high gene dosage can eliminate the temperature sensitive phenotype of the *E. coli* LJ14 cells [4]. However, since the amount of mutant RRF_{V117D} expressed by *E. coli* LJ14 cells (frr^{ts}) itself is much lower, which may be just enough for supporting bacterial cell growth at the permissive temperature, mutant RRF_{V117D} is inactivated by its cooperative unfolding at the non-permissive temperatures (at 42 and 45 °C) as shown in Fig. 5. Thus the residual activity of mutant RRF_{V117D} is not enough to support normal growth of the *E. coli* LJ14 cells at the non-permissive temperatures. This could explain why V117D substitution causes the temperature sensitive phenotype of the *E. coli* LJ14 cells.

Acknowledgments

We thank Professor A. Kaji, Department of Microbiology, School of Medicine, University of Pennsylvania, PA, USA for providing *E. coli* LJ14 and MRE600 strains. This work was supported by Grants (Nos. G1999075608 and 3017021) from the Chinese Committee for Science and Technology.

References

[1] D.V. Freistroffer, M.Y. Pavlov, J. MacDougall, R.H. Buckingham, M. Ehrenberg, EMBO J. 16 (1997) 4126–4133.
[2] A.V. Zavialov, R.H. Buckingham, M. Ehrenberg, Cell 107 (2001) 115–124.
[3] A.V. Zavialov, L. Mora, R.H. Buckingham, M. Ehrenberg, Mol. Cell 10 (2002) 789–798.
[4] L. Janosi, S. Mottagui-Tabar, L.A. Isaksson, Y. Sekine, E. Ohtsubo, S. Zhang, S. Goon, S. Nelken, M. Shuda, A. Kaji, EMBO J. 17 (1998) 1141–1151.
[5] T. Fujiwara, K. Ito, T. Nakayashiki, Y. Nakamura, FEBS Lett. 447 (1999) 297–302.
[6] L. Janosi, H. Hara, S. Zhang, A. Kaji, Adv. Biophys. 32 (1996) 121–201.
[7] L. Janosi, R. Ricker, A. Kaji, Biochimie 78 (1996) 959–969.
[8] M.Y. Pavlov, D. Freistroffer, J. MacDougall, R.H. Buckingham, M. Ehrenberg, EMBO J. 16 (1997) 4134–4141.
[9] R. Karimi, M.Y. Pavlov, R.H. Buckingham, M. Ehrenberg, Mol. Cell 3 (1999) 601–609.
[10] T. Toyoda, O.F. Tin, K. Ito, T. Fujiwara, T. Kumasaka, M. Yamamoto, M.B. Garber, Y. Nakamura, RNA 6 (2000) 1432–1444.
[11] H. Nakano, T. Yoshida, S. Uchiyama, M. Kawachi, H. Matsuo, T. Kato, A. Ohshima, Y. Yamaichi, T. Honda, H. Kato, Y. Yamagata, T. Ohkubo, Y. Kobayashi, J. Biol. Chem. 278 (2003) 3427–3436.
[12] M. Selmer, S. Al-Karadaghi, G. Hirokawa, A. Kaji, A. Liljas, Science 286 (1999) 2349–2352.
[13] K.K. Kim, K. Min, S.W. Suh, EMBO J. 19 (2000) 2362–2370.
[14] H. Nakano, S. Uchiyama, T. Yoshida, T. Ohkubo, H. Kato, Y. Yamagata, Y. Kobayashi, Acta Crystallogr. D Biol. 58 (2002) 124–126.
[15] T. Yoshida, S. Uchiyama, H. Nakano, H. Kashimori, H. Kijima, T. Ohshima, Y. Saihara, T. Ishino, H. Shimahara, T. Yoshida, K. Yokose, T. Ohkubo, A. Kaji, Y. Kobayashi, Biochemistry 40 (2001) 2387–2396.
[16] K. Saikrishnan, S.K. Kalapala, U. Varshney, M. Vijayan, J. Mol. Biol. 345 (2005) 29–38.

[17] L. Lancaster, M.C. Kiel, A. Kaji, H.F. Noller, Cell 111 (2002) 129–140.
[18] R.K. Agrawal, M.R. Sharma, M.C. Kiel, G. Hirokawa, T.M. Booth, C.M. Spahn, R.A. Grassucci, A. Kaji, J. Frank, Proc. Natl. Acad. Sci. USA 101 (2004) 8900–8905.
[19] T. Fujiwara, K. Ito, T. Yamami, Y. Nakamura, Mol. Microbiol. 53 (2004) 517–528.
[20] M.C. Kiel, V.S. Raj, H. Kaji, A. Kaji, J. Biol Chem. 278 (2003) 48041–48050.
[21] F. Peske, M.V. Rodnina, W. Wintermeyer, Mol. Cell 18 (2005) 403–412.
[22] A.V. Zavialov, V.V. Hauryliuk, M. Ehrenberg, Mol. Cell 18 (2005) 675–686.
[23] D.N. Wilson, F. Schluenzen, J.M. Harms, T. Yoshida, T. Ohkubo, R. Albrecht, J. Buerger, Y. Kobayashi, P. Fucini, EMBO J. 24 (2005) 251–260.
[24] N. Gao, A.V. Zavialov, W. Li, J. Sengupta, M. Valle, R.P. Gursky, M. Ehrenberg, J. Frank, Mol. Cell 18 (2005) 663–674.
[25] P. Guo, L.Q. Zhang, H.J. Zhang, Y.M. Feng, G.Z. Jing, Biochem. J. 393 (2006) 767–777.
[26] T. Yoshida, S. Oka, S. Uchiyama, H. Nakano, T. Kawasaki, T. Ohkubo, Y. Kobayashi, Biochemistry 42 (2003) 4101–4107.
[27] X.L. Zhang, P. Guo, G.Z. Jing, Biotech. Lett. 25 (2003) 755–760.
[28] P. Guo, L.Q. Zhang, Z. Qi, R.S. Chen, G.Z. Jing, J. Biochem. 138 (2005) 89–94.
[29] R. Higuchi, B. Krummel, R.K. Saiki, Nucleic Acids Res. 16 (1988) 7351–7367.
[30] C.N. Pace, F. Vajdos, L. Fee, G. Grimsley, T. Gray, Protein Sci. 4 (1995) 2411–2423.
[31] A.R. Rao, U. Varshney, EMBO J. 20 (2001) 2977–2986.
[32] C. Jatzke, H.-J. Hinz, U. Seedorf, G. Assmann, Biochim. Biophys. Acta 1432 (1999) 265–274.
[33] M.M. Santoro, D.W. Bolen, Biochemistry 27 (1988) 8063–8068.
[34] K.-C. Aune, C. Tanford, Biochemistry 8 (1969) 4586–4590.
[35] H. Eyring, J. Chem. Phys. 3 (1935) 107–115.
[36] Y.V. Griko, A. Gittis, E.E. Lattman, P.L. Privalov, J. Mol. Biol. 243 (1994) 93–99.
[37] H.J. Zhang, S. Huang, Y.M. Feng, P. Guo, G.Z. Jing, Arch. Biochem. Biophys. 441 (2005) 123–131.
[38] V. Clément-Collin, A. Barbier, A.D. Dergunov, A. Visvikis, G. Siest, M. Desmadril, M. Takahashi, L.P. Aggerbeck, Biophys. chem. 119 (2006) 170–185.
[39] S. Benjwal, S. Verma, K.-H. Rohm, O. Gursky, Protein Sci. 15 (2006) 635–639.
[40] J.K. Myers, C.N. Pace, J.M. Scholtz, Protein Sci. 4 (1995) 2138–2148.
[41] N. Schoenbrunner, K.-P. Koller, T. Kiefhaber, J. Mol. Biol. 268 (1997) 526–538.